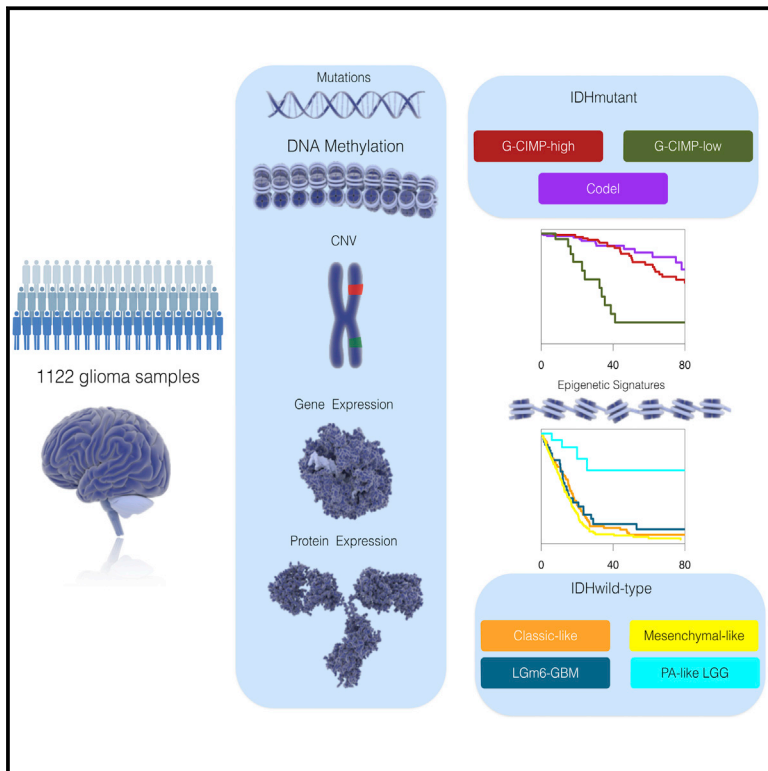


Molecular Profiling Reveals Biologically Discrete Subsets and Pathways of Progression in Diffuse Glioma

Graphical Abstract



Authors

Michele Ceccarelli, Floris P. Barthel, Tathiane M. Malta, ..., Houtan Noushmehr, Antonio Iavarone, Roel G.W. Verhaak

Correspondence

houtan@usp.br (H.N.),
ai2102@columbia.edu (A.I.),
rverhaak@mdanderson.org (R.G.W.V.)

In Brief

Integration of a large sample size of glioma tumors with multidimensional ‘omic characterization and clinical annotation provides insights into molecular classification, telomere maintenance mechanisms, progression from low to high grade disease, driver mutations, and therapeutic options.

Highlights

- Comprehensive molecular profiling of 1,122 adult diffuse grade II, III, and IV gliomas
- Telomere length and telomere maintenance defined by somatic alterations
- DNA methylation profiling reveals subtypes of IDH mutant and IDH-wild-type glioma
- Integrated molecular analysis of progression from low-grade to high-grade disease



Molecular Profiling Reveals Biologically Discrete Subsets and Pathways of Progression in Diffuse Glioma

Michele Ceccarelli,^{1,2,24} Floris P. Barthel,^{3,4,24} Tathiane M. Malta,^{5,6,24} Thais S. Sabedot,^{5,6,24} Sofie R. Salama,⁷ Bradley A. Murray,⁸ Olena Morozova,⁷ Yulia Newton,⁷ Amie Radenbaugh,⁷ Stefano M. Pagnotta,^{2,9} Samreen Anjum,¹ Jiguang Wang,¹⁰ Ganiraju Manyam,³ Pietro Zoppoli,¹⁰ Shiyun Ling,³ Arjun A. Rao,⁷ Mia Grifford,⁷ Andrew D. Cherniack,⁸ Hailei Zhang,⁸ Laila Poisson,¹¹ Carlos Gilberto Carlotti, Jr.,^{5,6} Daniela Pretti da Cunha Tirapelli,^{5,6} Arvind Rao,³ Tom Mikkelsen,¹¹ Ching C. Lau,^{12,13} W.K. Alfred Yung,³ Raul Rabadan,¹⁰ Jason Huse,¹⁴ Daniel J. Brat,¹⁵ Norman L. Lehman,¹⁶ Jill S. Barnholtz-Sloan,¹⁷ Siyuan Zheng,³ Kenneth Hess,³ Ganesh Rao,³ Matthew Meyerson,^{8,18} Rameen Beroukhi,^{8,18,19} Lee Cooper,¹⁵ Rehan Akbani,³ Margaret Wrensch,²⁰ David Haussler,⁷ Kenneth D. Aldape,²¹ Peter W. Laird,²² David H. Gutmann,²³ TCGA Research Network, Houtan Noushmehr,^{5,6,25,*} Antonio Iavarone,^{10,25,*} and Roel G.W. Verhaak^{3,25,*}

¹Qatar Computing Research Institute, Hamad Bin Khalifa University, Doha P.O. box 5825, Qatar

²Department of Science and Technology, University of Sannio, Benevento 82100, Italy

³Department of Genomic Medicine, Department of Bioinformatics and Computational Biology, Department of Biostatistics, Department of Neuro-Oncology, Department of Neurosurgery, Department of Pathology, University of Texas MD Anderson Cancer Center, Houston, TX 77030, USA

⁴Oncology Graduate School Amsterdam, Department of Pathology, VU University Medical Center, 1081 HV Amsterdam, the Netherlands

⁵Department of Genetics (CISBi/NAP), Department of Surgery and Anatomy, Ribeirão Preto Medical School, University of São Paulo, Monte Alegre, Ribeirão Preto-SP CEP: 14049-900, Brazil

⁶Center for Integrative Systems Biology (CISBi, NAP/USP), Ribeirão Preto Medical School, University of São Paulo, Ribeirão Preto, São Paulo 14049-900, Brazil

⁷UC Santa Cruz Genomics Institute, University of California, Santa Cruz, Santa Cruz, CA 95064, USA

⁸The Eli and Edythe L. Broad Institute of Massachusetts Institute of Technology and Harvard University, Cambridge, MA 02142, USA

⁹BIOGEM Istituto di Ricerche Genetiche "G. Salvatore," Campo Reale, 83031 Ariano Irpino, Italy

¹⁰Department of Neurology, Department of Pathology, Institute for Cancer Genetics, Department of Systems Biology and Biomedical Informatics, Columbia University Medical Center, New York, NY 10032, USA

¹¹Henry Ford Hospital, Detroit, MI 48202, USA

¹²Texas Children's Hospital, Houston, TX 77030, USA

¹³Baylor College of Medicine, Houston, TX 77030, USA

¹⁴Memorial Sloan Kettering Cancer Center, New York, NY 10065, USA

¹⁵Winship Cancer Institute, Emory University, Atlanta, GA 30322, USA

¹⁶Department of Pathology, The Ohio State University, Columbus, OH 43210, USA

¹⁷Case Comprehensive Cancer Center, Case Western Reserve University, Cleveland, OH 44106, USA

¹⁸Department of Medical Oncology, Dana-Farber Cancer Institute, Boston, MA 02215, USA

¹⁹Department of Medicine, Harvard Medical School, Boston, MA 02215, USA

²⁰Department of Neurological Surgery, University of California, San Francisco, San Francisco, CA 94158, USA

²¹Princess Margaret Cancer Centre, Toronto, ON M5G 2M9, Canada

²²Van Andel Research Institute, Grand Rapids, MI 49503, USA

²³School of Medicine, Washington University, St. Louis, MO 63110, USA

²⁴Co-first author

²⁵Co-senior author

*Correspondence: houtan@usp.br (H.N.), ai2102@columbia.edu (A.I.), rverhaak@mdanderson.org (R.G.W.V.)
<http://dx.doi.org/10.1016/j.cell.2015.12.028>

SUMMARY

Therapy development for adult diffuse glioma is hindered by incomplete knowledge of somatic glioma driving alterations and suboptimal disease classification. We defined the complete set of genes associated with 1,122 diffuse grade II-III-IV gliomas from The Cancer Genome Atlas and used molecular profiles to improve disease classification, identify molecular correlations, and provide insights into

the progression from low- to high-grade disease. Whole-genome sequencing data analysis determined that *ATRX* but not *TERT* promoter mutations are associated with increased telomere length. Recent advances in glioma classification based on *IDH* mutation and 1p/19q co-deletion status were recapitulated through analysis of DNA methylation profiles, which identified clinically relevant molecular subsets. A subtype of *IDH* mutant glioma was associated with DNA demethylation and poor outcome;

a group of IDH-wild-type diffuse glioma showed molecular similarity to pilocytic astrocytoma and relatively favorable survival. Understanding of cohesive disease groups may aid improved clinical outcomes.

INTRODUCTION

Diffuse gliomas represent 80% of malignant brain tumors (Schwartzbaum et al., 2006). Adult diffuse gliomas are classified and graded according to histological criteria (oligodendroglioma, oligoastrocytoma, astrocytoma, and glioblastoma; grade II to IV). Although histopathologic classification is well established and is the basis of the World Health Organization (WHO) classification of CNS tumors (Louis et al., 2007), it suffers from high intra- and inter-observer variability, particularly among grade II-III tumors (van den Bent, 2010). Recent molecular characterization studies have benefited from the availability of the datasets generated by The Cancer Genome Atlas (TCGA) (Brennan et al., 2013; Eckel-Passow et al., 2015; Frattini et al., 2013; Kim et al., 2015; Suzuki et al., 2015; Cancer Genome Atlas Research Network et al., 2015) and have related genetic, gene expression, and DNA methylation signatures with prognosis (Noushmehr et al., 2010; Sturm et al., 2012; Verhaak et al., 2010). For example, mutations in the isocitrate dehydrogenase genes 1 and 2 (*IDH1/IDH2*) define a distinct subset of glioblastoma (GBM) with a hypermethylation phenotype (G-CIMP) with favorable outcome (Noushmehr et al., 2010; Yan et al., 2009). Conversely, the absence of *IDH* mutations in LGG marks a distinct IDH-wild-type subgroup characterized by poor, GBM-like prognosis (Eckel-Passow et al., 2015; Cancer Genome Atlas Research Network et al., 2015). Recent work by us and others has proposed classification of glioma into *IDH* wild-type cases, *IDH* mutant group additionally carrying codeletion of chromosome arm 1p and 19q (*IDH* mutant-codel) and samples with euploid 1p/19q (*IDH* mutant-non-codel), regardless of grade and histology (Eckel-Passow et al., 2015; Cancer Genome Atlas Research Network et al., 2015). Mutation of the *TERT* promoter, which has been reported with high frequency across glioma, may be an additional defining feature. Current analyses have not yet clarified the relationships between LGGs and GBMs that share common genetic hallmarks like *IDH* mutation or *TERT* promoter mutation status. An improved understanding of these relationships will be necessary as we evolve toward an objective genome-based clinical classification.

To address the above issues, we assembled a dataset comprising all TCGA newly diagnosed diffuse glioma consisting of 1,122 patients and comprehensively analyzed using sequencing and array-based molecular profiling approaches. We have addressed crucial technical challenges in analyzing this comprehensive dataset, including the integration of multiple platforms and data sources (e.g., multiple methylation and gene expression platforms). We identified new diffuse glioma subgroups with distinct molecular and clinical features and shed light on the mechanisms driving progression of lower grade glioma (LGG) (WHO grades II and III) into full-blown GBM (WHO grade IV).

RESULTS

Patient Cohort Characteristics

The TCGA LGG and GBM cohorts consist of 516 and 606 patients, respectively. Independent analysis of the GBM dataset was previously described, as was analysis of 290 LGG samples (Brennan et al., 2013; Cancer Genome Atlas Research Network et al., 2015). 226 LGG samples were added to our current cohort (Table 1). Clinical data, including age, tumor grade, tumor histology, and survival, were available for 93% (1,046/1,122) of cases (Table S1). The majority of samples were grade IV tumors (n = 590, 56%), whereas 216 (21%) and 241 (23%) were grade II and III tumors, respectively. Similarly, 590 (56%) samples were classified as GBM, 174 (17%) as oligodendroglioma, 169 (16%) as astrocytoma, and 114 (11%) as oligoastrocytoma.

Among the data sources considered in our analysis were gene expression (n = 1,045), DNA copy number (n = 1,084), DNA methylation (n = 932), exome sequencing (n = 820), and protein expression (n = 473). Multiple and overlapping characterization assays were employed (Table S1). All data files that were used in our analysis can be found at https://tcga-data.nci.nih.gov/docs/publications/lgggbm_2015/.

Identification of Novel Glioma-Associated Genomic Alterations

To establish the set of genomic alterations that drive gliomagenesis, we called point mutations and indels on the exomes of 513 LGG and 307 GBM using the Mutect, Indelocator, Varscan2, and RADIA algorithms and considered all mutations identified by at least two callers. Significantly mutated genes (SMGs) were determined using MutSigCV. This led to the identification of 75 SMGs, 10 of which had been previously reported in GBM (Brennan et al., 2013), 12 of which had been reported in LGG (Cancer Genome Atlas Research Network et al., 2015), and 8 of which had been identified in both GBM and LGG studies. 45 SMGs have not been previously associated with glioma and ranged in mutation frequency from 0.5% to 2.6% (Table S2A). We used GISTIC2 to analyze the DNA copy number profiles of 1,084 samples, including 513 LGG and 571 GBM, and identified 162 significantly altered DNA copy number segments (Table S2B). We employed PRADA and deFuse to detect 1,144 gene fusion events in the RNA-seq profiles available for 154 GBM and 513 LGG samples, of which 37 in-frame fusions involved receptor tyrosine kinases (Table S2C). Collectively, these analyses recovered all known glioma driving events, including in *IDH1* (n = 457), *TP53* (n = 328), *ATRX* (n = 220), *EGFR* (n = 314), *PTEN* (n = 168), *CIC* (n = 80), and *FUBP1* (n = 45). Notable newly predicted glioma drivers relative to the earlier TCGA analyses were genes associated with chromatin organization such as *SETD2* (n = 24), *ARID2* (n = 20), *DNMT3A* (n = 11), and the *KRAS/NRAS* oncogenes (n = 25 and n = 5, respectively).

We overlapped copy number, mutation (n = 793), and fusion transcript (n = 649) profiles and confirmed the convergence of genetic drivers of glioma into pathways, including the Ras-Raf-MEK-ERK, p53/apoptosis, PI3K/AKT/mTOR, chromatin modification, and cell cycle pathways. The Ras-Raf-MEK-ERK signaling cascade showed alterations in 106 of 119 members

Table 1. Clinical Characteristics of the Sample Set Arranged by IDH and 1p/19q Co-deletion Status

Feature	IDH Wt (n = 520)	IDH mut - non-codel (n = 283)	IDH mut - codel (n = 171)	Unknown (n = 148)
Clinical				
Histology (n)				
Astrocytoma	52 (10.0%)	112 (39.6%)	4 (2.3%)	1 (0.7%)
Glioblastoma	419 (80.6%)	32 (11.3%)	2 (1.2%)	137 (92.6%)
Oligoastrocytoma	15 (2.9%)	69 (24.4%)	30 (17.5%)	0 (0%)
Oligodendroglioma	19 (3.7%)	37 (13.1%)	117 (68.4%)	1 (0.7%)
Unknown	15 (2.9%)	33 (11.7%)	18 (10.5%)	9 (6.1%)
Grade (n)				
G2	19 (3.7%)	114 (40.3%)	81 (47.4%)	2 (1.4%)
G3	67 (12.9%)	104 (36.7%)	70 (40.9%)	0 (0%)
G4	419 (80.6%)	32 (11.3%)	2 (1.2%)	137 (92.6%)
Unknown	15 (2.9%)	33 (11.7%)	18 (10.5%)	9 (6.1%)
Age				
Median (LQ-UQ)	59 (51–68)	38 (30–44)	46 (35–54)	55 (48–68)
Unknown (n)	16	33	18	9
Survival				
Median (CI)	14.0 (12.6–15.3)	75.1 (62.1–94.5)	115.8 (90.5–Inf)	12.6 (11.3–14.9)
Unknown (n)	14	32	18	12
KPS				
<70	85 (16.3%)	8 (2.8%)	5 (2.9%)	21 (14.2%)
70–80	196 (37.7%)	41 (14.5%)	18 (10.5%)	60 (40.5%)
90	29 (5.6%)	60 (21.2%)	32 (18.7%)	2 (1.4%)
100	51 (9.8%)	44 (15.9%)	30 (17.5%)	14 (9.5%)
Unknown	159 (30.6%)	129 (45.6%)	86 (50.3%)	51 (34.5%)
Molecular				
MGMT promoter				
Methylated	170 (32.7%)	242 (85.5%)	169 (98.8%)	32 (21.6%)
Unmethylated	248 (47.7%)	36 (12.7%)	1 (0.6%)	34 (23.0%)
Unknown	102 (19.6%)	5 (1.8%)	1 (0.6%)	82 (55.4%)
TERT promoter				
Mutant	67 (12.9%)	8 (2.8%)	86 (50.3%)	1 (0.7%)
Wild-type	19 (9.8%)	146 (51.6%)	2 (1.2%)	0 (0%)
Unknown	434 (83.5%)	129 (45.6%)	83 (48.5%)	135 (99.3%)
TERT expression				
Expressed	178 (34.2%)	14 (4.9%)	153 (89.5%)	6 (4.1%)
Not expressed	51 (9.8%)	242 (85.5%)	16 (9.4%)	7 (4.7%)
Unknown	291 (56.0%)	27 (9.5%)	2 (1.2%)	135 (91.2%)

detected across 578 cases (73%), mostly occurring in IDH-wild-type samples (n = 327 of 357, 92%). Conversely, we found that a set of 36 genes involved in chromatin modification was targeted by genetic alterations in 423 tumors (54%, n = 36 genes), most of which belonged to the IDH mutant-non-codel group (n = 230, 87%).

In order to identify new somatically altered glioma genes, we used MutComFocal to nominate candidates altered by mutation, as well as copy number alteration. Prominent among these genes was *NIPBL*, a crucial adherin subunit that is essential for loading cohesins on chromatin (Table S2D) (Peters and Nish-

iyama, 2012). The cohesin complex is responsible for the adhesion of sister chromatids following DNA replication and is essential to prevent premature chromatid separation and faithful chromosome segregation during mitosis (Peters and Nishiyama, 2012). Alterations in the cohesin pathway have been reported in 12% of acute myeloid leukemias (Kon et al., 2013). Mutations of the cohesin complex gene *STAG2* had been previously reported in GBM (Brennan et al., 2013). Taken together, 16% of the LGG/GBM showed mutations and/or CNAs in multiple genes involved in the cohesin complex, thus nominating this process as a prominent pathway involved in gliomagenesis.

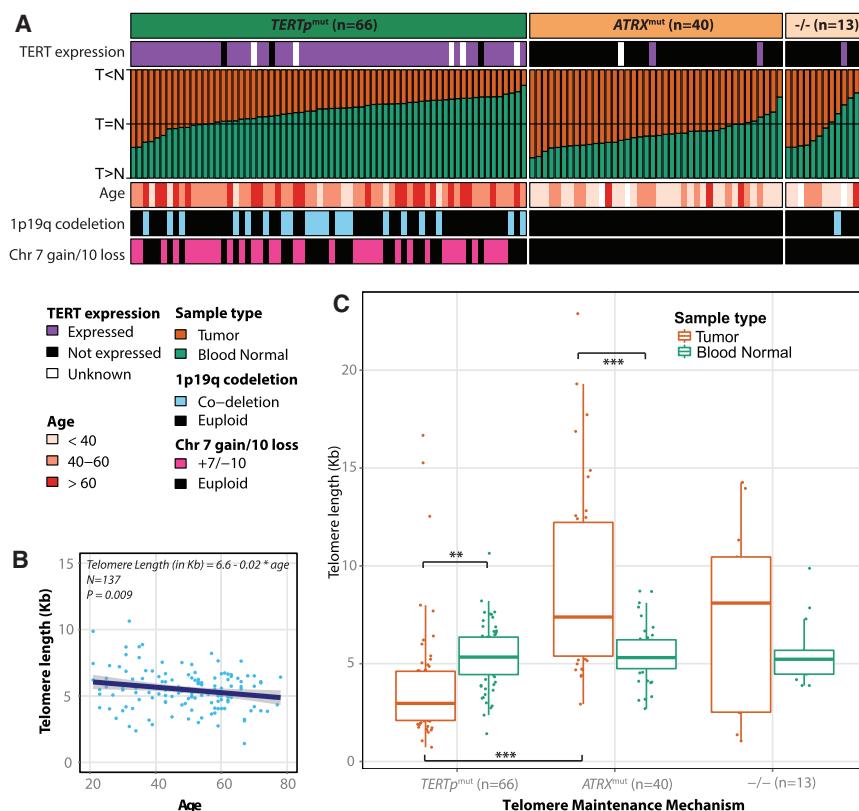


Figure 1. Telomere Length Associations in Glioma

(A) Heatmap of relative tumor/normal telomere lengths of 119 gliomas, grouped by *TERTp* and *ATRX* mutation status.

(B) Telomere length decreases with increasing age (measured in years at diagnosis) in blood normal control samples (n = 137).

(C) Quantitative telomere length estimates of tumors and blood normal, grouped by *TERTp* mutant (n = 67, 56%), *ATRX* mutant (n = 40, 33%), and double negative (n = 13, 11%) status. *** = p < 0.0001; ** = p < 0.001.

Telomere Length Is Positively Correlated with *ATRX*, but Not *TERT* Promoter Mutations

Mutations in the *TERT* promoter (*TERTp*) have been reported in 80% of GBM (Killela et al., 2013). We used *TERTp* mutation calls from targeted sequencing (n = 287) and complemented them with *TERTp* mutations inferred from whole-genome sequencing (WGS) data (n = 42). *TERTp* mutations are nearly mutually exclusive with mutations in *ATRX* (Eckel-Passow et al., 2015), which was confirmed in our cohort. Overall, 85% of diffuse gliomas harbored mutations of *TERTp* (n = 157, 48%) or *ATRX* (n = 120, 37%). *TERTp* mutations activate *TERT* mRNA expression through the creation of a de novo E26 transformation-specific (ETS) transcription factor-binding site (Horn et al., 2013), and we observed significant *TERT* upregulation in *TERTp* mutant cases (p value < 0.0001, Figure S1A). *TERT* expression measured by RNA-seq was a highly sensitive (91%) and specific (95%) surrogate for the presence of *TERTp* mutation (Figure S1B). We correlated *TERTp* status with glioma driving alterations and observed that nearly all IDH-wild-type cases with chromosome 7 gain and chromosome 10 loss harbored *TERTp* mutations or upregulated *TERT* expression (n = 52/53 and n = 134/147, respectively; Figure 1A). Conversely, only 45% of IDH-wild-type samples lacking chromosome 7/chromosome 10 events showed *TERTp* mutations or elevated *TERT* expression (n = 15/33 and n = 43/82, respectively). Thus, *TERTp* mutations may precede the chr 7/chr 10 alterations that have been implicated in glioma initiation (Ozawa et al., 2014).

To correlate *TERTp* mutations to telomere length, we used whole-genome sequencing and low pass whole-genome sequencing data to estimate telomere length in 141 pairs of matched tumor and normal samples. As expected, we observed an inverse correlation of telomere length with age at diagnosis in matching blood normal samples (Figure 1B) and tumor samples (Figure S1C). Glioma samples harboring *ATRX* mutations showed significantly longer telomeres compared to *TERTp* mutant samples (t test p value < 0.0001; Figure 1C). Among *TERTp* mutation gliomas, there

was no difference in telomere length between samples with and without additional *IDH1/IDH2* mutations, despite a difference in age. *ATRX* forms a complex with DAXX and H3.3, and the genes encoding these proteins are frequently mutated in pediatric gliomas (Sturm et al., 2012). Mutations in DAXX and H3F3A were identified in only two samples in our WGS dataset. The *ATRX*-DAXX-H3.3 complex is associated with the alternative lengthening of telomeres (ALT) and our observations confirm previously hypothesized fundamental differences between the telomere control exerted by telomerase and ALT (Sturm et al., 2014).

As demonstrated by the identification of *TERTp* mutations, somatic variants affecting regulatory regions may play a role in gliomagenesis. Using 67 matched whole-genome and RNA-seq expression pairs, we similarly sought to identify mutations located within 2 kb upstream of transcription start sites and associated with a gene expression change. Using strict filtering methods, we identified 12 promoter regions with mutations in at least 6 samples. Three of 12 regions related to a significant difference in the expression of the associated gene expression, suggesting possible functional consequences. Other than *TERT* (n = 37), promoter mutations of the ubiquitin ligase *TRIM28* (n = 8) and the calcium channel gamma subunit *CACNG6* (n = 7) correlated with respectively upregulation and downregulation of these genes, respectively (Table S2E). *TRIM28* has been reported to mediate the ubiquitin-dependent degradation of AMP-activated protein kinase (AMPK) leading to activation of mTOR signaling and hypersensitization to AMPK agonists, such as metformin (Pineda et al., 2015).

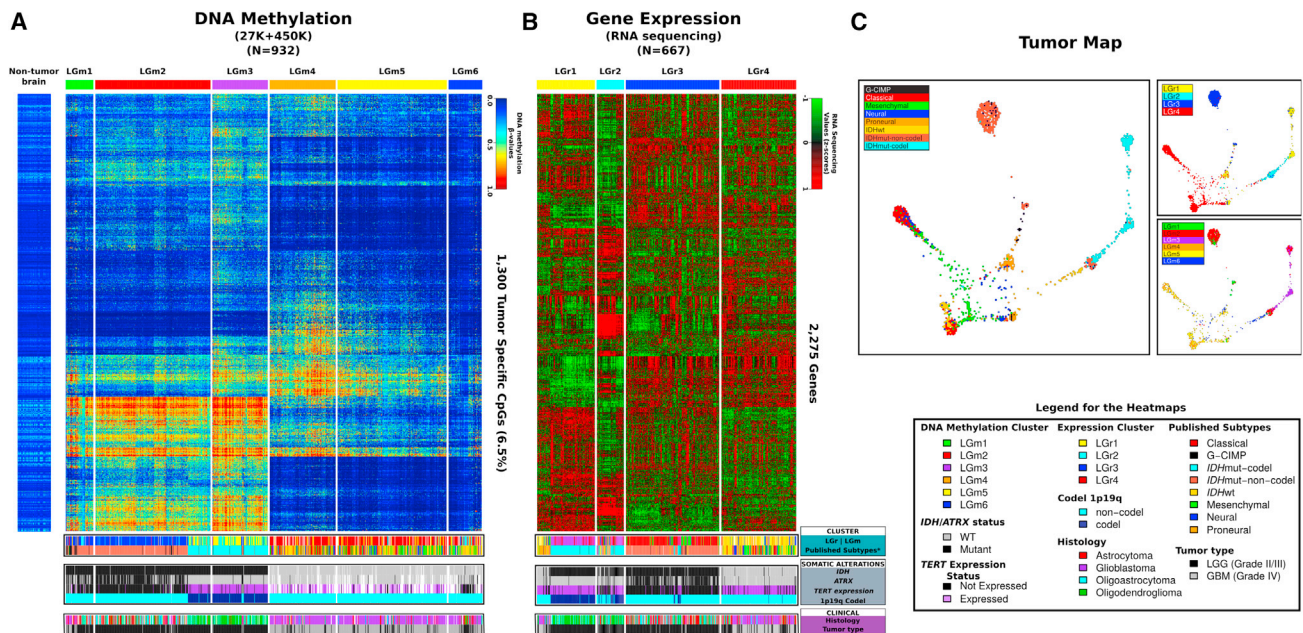


Figure 2. Pan-glioma DNA Methylation and Transcriptome Subtypes

(A) Heatmap of DNA methylation data. Columns represent 932 TCGA glioma samples grouped according to unsupervised cluster analysis; rows represent DNA methylation probes sorted by hierarchical clustering. Non-neoplastic samples are represented on the left of the heatmap ($n = 77$) (Guintivano et al., 2013).

(B) Heatmap of RNA sequencing data. Unsupervised clustering analysis for 667 TCGA glioma samples profiled using RNA sequencing are plotted in the heatmap using 2,275 most variant genes. Previously published subtypes were derived from Brennan et al. (2013) and Cancer Genome Atlas Research Network et al., 2015.

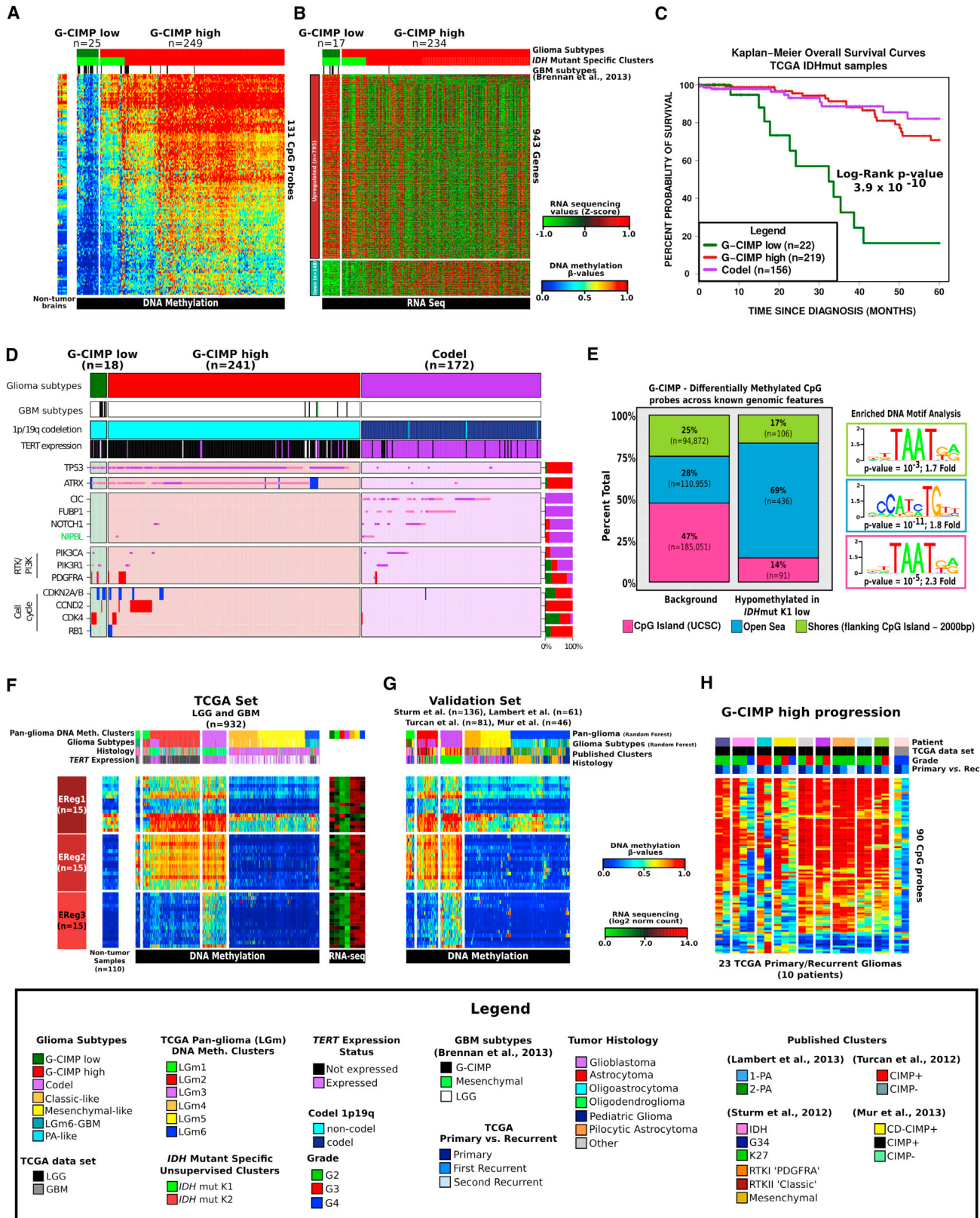
(C) Tumor Map based on mRNA expression and DNA methylation data. Each data point is a TCGA sample colored coded according to their identified status. A live interactive version of this map is available at <http://tumormap.ucsc.edu/?p=ynewton.gliomas-paper>.

Unsupervised Clustering of Gliomas Identifies Six Methylation Groups and Four RNA Expression Groups Associated with IDH Status

To segregate the DNA methylation subtypes across the pan-glioma dataset, we analyzed 932 glioma samples profiled on the HumanMethylation450 platform (516 LGG and 129 GBM) and the HumanMethylation27 platform (287 GBM). In order to incorporate the maximum number of samples, we merged datasets from both methylation platforms yielding a core set of 25,978 CpG probes. To reduce computational requirements to cluster this large dataset, we eliminated sites that were methylated (mean β value ≥ 0.3) in non-tumor brain tissues and selected 1,300 tumor-specific methylated probes (1,300/25,978, 5%) to perform unsupervised k-means consensus clustering. This identified six distinct clusters, labeled LGM1–6 (Figure 2A and Tables S1 and S3A). Next, we sought to determine pan-glioma expression subtypes through unsupervised clustering analysis of 667 RNA-seq profiles (513 LGG and 154 GBM), which resulted in four main clusters labeled LGr1–4 (Figure 2B and Tables S1 and S3A). An additional 378 GBM samples with Affymetrix HT-HG-U133A profiles (but lacking RNA-seq data) were classified into the four clusters using a k-nearest neighbor classification procedure. *IDH* mutation status was the primary driver of methylation and transcriptome clustering and separated the cohort into two macro-groups. The LGM1/LGM2/LGM3 DNA methylation macro-group carried *IDH1* or *IDH2* mutations (449 of 450, 99%) and was enriched for LGG (421/454, 93%) while LGM4/

LGM5/LGM6 were *IDH*-wild-type (429/430, 99%) and enriched for GBM (383/478, 80%). LGM1–3 showed genome-wide hypermethylation compared to LGM4–6 clusters (Figure S2A), documenting the association between *IDH* mutation and increased DNA methylation (Noushmehr et al., 2010; Turcan et al., 2012). Principal component analysis using 19,520 probes yielded similar results, thus emphasizing that our probe selection method did not introduce unwanted bias (Figure S2B). The gene expression clusters LGr1–3 harbored *IDH1* or *IDH2* mutations (438 of 533, 82%) and were enriched for LGG (436/563, 77%), while the LGr4 was exclusively *IDH*-wild-type (376 of 387, 97%) and enriched for GBM (399/476, 84%).

We extended our analysis using Tumor Map (Supplemental Experimental Procedures) to perform integrated co-clustering analysis of the combined gene expression ($n = 1,196$) and DNA methylation ($n = 867$) profiles. An interactive Tumor Map version is publicly available at <http://tumormap.ucsc.edu/?p=ynewton.gliomas-paper>. Tumor Map assigns samples to a hexagon in a grid so that nearby samples are likely to have similar genomic profiles and allows visualizing complex relationships between heterogeneous genomic data samples and their clinical or phenotypical associations. Thus, clusters in the map indicate groups of samples with high similarity of integrated gene expression and DNA methylation profiles (Figure 2C). The map confirms clustering by *IDH* status and additionally shows islands of samples that share previously reported GBM cluster memberships (Noushmehr et al., 2010; Verhaak et al., 2010). To assess



(legend on next page)

clustering sensitivity to pre-processing, we tried complementary methods and obtained similar results (Figure S2C).

To identify genes whose copy number changes are associated with concordant changes in gene expression, we combined expression and copy number profiles from 659 samples to define a signature of 57 genes with strong functional copy number (fCN) change (Table S3B). The fCN signature clustered gliomas into three macro-clusters, LGfc1–3, strongly associated with IDH and 1p/19q status (Figure S2D). The fCN analysis revealed the functional activation of a cluster of *HOXA* genes in the IDH-wild-type LGfc2 cluster, which were previously associated with glioma stem cell maintenance (Kurscheid et al., 2015).

Finally, we clustered reverse phase protein array profiles, consisting of 196 antibodies on 473 samples. Two macro clusters were observed, and in contrast to the transcriptome/methylome/fCNV clustering, the primary discriminator was based on glioma grade (LGG versus GBM) rather than IDH status (Figure S2E). Compared to the LGG-like cluster, the GBM-like cluster had elevated expression of IGFBP2, fibronectin, PAI1, HSP70, EGFR, phosphoEGFR, phosphoAKT, Cyclin B1, Caveolin, Collagen VI, Annexin1, and ASNS, whereas the LGG class showed increased activity of PKC (alpha, beta, and delta), PTEN, BRAF, and phosphoP70S6K.

The above results confirm IDH status as the major determinant of the molecular footprints of diffuse glioma. To further elucidate the subtypes of diffuse glioma, we performed unsupervised clustering within each of the two IDH-driven macroclusters. We used 1,308 tumor-specific CpG probes defined among the IDH mutation cohort ($n = 450$) and identified three IDH mutant-specific DNA methylation clusters (Figure S3A). Using 914 tumor-specific CpG probes in the IDH-wild-type cohort ($n = 430$), we uncovered three IDH-wild-type-specific clusters (Figure S4A). The sets of CpG probes used to cluster each of the two IDH-driven datasets overlapped significantly with the 1,300 probes that defined the pan-glioma DNA methylation clustering (1162/1,300, 89% and 853/1,300, 66%, for IDH mutant and IDH-wild-type, respectively). The clusters identified by separating IDH mutant and IDH-wild-type gliomas showed strong overall concordance with pan-glioma DNA methylation subtypes (Table S3A). Similarly, unsupervised clustering of 426 IDH mutant RNA-seq profiles resulted in three subtypes (Figure S3A), and analysis of the 234 IDH-wild-type samples led to four mixed LGG/GBM clusters that showed enrichment for previously identified GBM expression subtypes (Figure S4C) (Verhaak et al., 2010).

An Epigenetic Signature Associated with Activation of Cell Cycle Genes Segregates a Subgroup of IDH Mutant LGG and GBM with Unfavorable Clinical Outcome

The three epigenetic subtypes defined by clustering IDH mutant glioma separated samples harboring the 1p/19q co-deletion into a single cluster and non-codel glioma into two clusters (Figure S3A). Conversely, non-codel glioma grouped nearly exclusively into a single expression cluster, and codels were split in two separated expression clusters (Figure S3A). A distinct subgroup of samples within the IDH mutant-non-codel DNA methylation clusters manifested relatively reduced DNA methylation (Figure S3B). The unsupervised clustering of IDH mutant glioma was unable to segregate the lower methylated non-codel subgroup as the 1,308 probes selected for unsupervised clustering included only 19 of the 131 differentially methylated probes characteristic for this subgroup ($FDR < 10^{-15}$, difference in mean methylation beta value > 0.27). The low-methylation subgroup consisted of both G-CIMP GBM (13/25) and LGGs (12/25) and was confirmed using a non-TCGA dataset (Figure S3C). The tumors with higher methylation in the split cluster were very similar to those grouped in the second non-codel cluster, and a supervised comparison identified only 12 probes as differentially DNA methylated (Figures 3A and 3B). We concluded that IDH mutant glioma is composed of three coherent subgroups: (1) the Codel group, consisting of IDH mutant-codel LGGs; (2) the G-CIMP-low group, including IDH mutant-non-codel glioma (LGG and GBM) manifesting relatively low genome-wide DNA methylation; and (3) the G-CIMP-high group, including IDH mutant-non-codel glioma (LGG and GBM) with higher global levels of DNA methylation. The newly identified G-CIMP-low group of glioma was associated with significantly worse survival as compared to the G-CIMP-high and Codel groups (Figure S3D). The clinical outcome of the tumors classified as G-CIMP-high was as favorable as that of Codel tumors, the subgroup generally thought to have the best prognosis among glioma patients (Figures 3C and S3D). We compared the frequencies of glioma driver gene alterations between the three types of IDH mutant glioma and found that 15 of 18 G-CIMP-low cases carried abnormalities in cell cycle pathway genes such as *CDK4* and *CDKN2A*, relative to 36/241 and 2/172 for G-CIMP-high and Codels, respectively (Figure 3D). Supervised analysis between gene expression of G-CIMP-low and G-CIMP-high resulted in 943 differentially expressed genes. We mapped the 943 deregulated genes to 767 nearest CpG probes (max distance 1 kb) and found the majority

Figure 3. Identification of a Distinct G-CIMP Subtype Defined by Epigenomics

- (A) Heatmap of probes differentially methylated between the two IDH mutant-non-codel DNA methylation clusters allowed the identification of a low-methylation subgroup named G-CIMP-low. Non-tumor brain samples ($n = 12$) are represented on the left of the heatmap.
- (B) Heatmap of genes differentially expressed between the two IDH mutant-non-codel DNA methylation clusters.
- (C) Kaplan-Meier survival curves of IDH mutant methylation subtypes. Ticks represent censored values.
- (D) Distribution of genomic alterations in genes frequently altered in IDH mutant glioma.
- (E) Genomic distribution of 633 CpG probes differentially demethylated between co-clustered G-CIMP-low and G-CIMP-high. CpG probes are grouped by UCSC genome browser-defined CpG Islands, shores flanking CpG island ± 2 kb and open seas (regions not in CpG islands or shores).
- (F) DNA methylation heatmap of TCGA glioma samples ordered per Figure 2A and the epigenetically regulated (EReg) gene signatures defined for G-CIMP-low, G-CIMP-high, and Codel subtypes. The mean RNA sequencing counts for each gene matched to the promoter of the identified cgID across each cluster are plotted to the right.
- (G) Heatmap of the validation set classified using the random forest method applying the 1,300 probes defined in Figure 2A.
- (H) Heatmap of probes differentially methylated between G-CIMP-low and G-CIMP-high in longitudinally matched tumor samples.

of the CpG probes (486/767, 63%) to show a significant methylation difference (FDR < 0.05, difference in mean methylation beta value > 0.01) between G-CIMP-low and G-CIMP-high, suggesting a mechanistic relation between loss of methylation and increased transcript levels.

Recent analysis of epigenetic profiles derived from colon cancers showed that transcription factors may bind to regions of demethylated DNA (Berman et al., 2012). Therefore, we asked whether transcription factors may be recruited to the DNA regions differentially methylated between G-CIMP-low samples and G-CIMP-high samples from the same methylation cluster, using 450K methylation profiles (n = 39). Globally, we detected 643 differentially methylated probes between 27 G-CIMP-low and 12 G-CIMP-high samples (absolute diff-mean difference ≥ 0.25 , FDR $\leq 5\%$). Most of these probes (69%) were located outside of any known CpG island but positioned within intergenic regions known as open seas (Figure 3E). This represents a 2.5-fold open sea enrichment compared to the expected genome-wide distribution of 450K CpG probes (chi-square p value < 2.2×10^{-16}). We also observed a 3.4-fold depletion within CpG islands (chi-square p value < 2.2×10^{-16}).

Using this set of intergenic CpG probes, we asked whether a DNA motif signature associated with distal regulatory elements. Such a pattern would point to candidate transcription factors involved in tumorigenesis of the G-CIMP-low group. A de novo motif scan and known motif scan identified a distinct motif signature TGTT (geometric test p value = 10^{-11} , fold enrichment = 1.8), known to be associated with the OLIG2 and SOX transcription factor families (Figure 3E) (Lodato et al., 2013). This observation was corroborated by the higher expression levels of SOX2, as well as 17 out of 20 other known SOX family members in G-CIMP-low compared to G-CIMP-high (fold difference > 2). The primary function of SOX2 in the nervous system is to promote self-renewal of neural stem cells and, within brain tumors, the glioma stem cell state (Graham et al., 2003). Interestingly, SOX2 and OLIG2 have been described as neurodevelopmental transcription factors being essential for GBM propagation (Suvà et al., 2014). Supervised gene expression pathway analysis of the genes activated in the G-CIMP-low group as opposed to G-CIMP-high group revealed activation of genes involved in cell cycle and cell division consistent with the role of SOX in promoting cell proliferation (Figure S3E). The enrichment in cell cycle gene expression provides additional support to the notion that development of the G-CIMP-low subtype is associated with activation of cell cycle progression and may be mediated by a loss of CpG methylation and binding of SOX factors to candidate genomic enhancer elements.

To validate the G-CIMP-low, G-CIMP-high, and Codel IDH mutant subtypes, we compiled a validation cohort from published studies, including 324 adult and pediatric gliomas (Lambert et al., 2013; Mur et al., 2013; Sturm et al., 2012; Turcan et al., 2012). The CpG probe methylation signatures used to classify the validation set are provided on the publication portal accompanying this publication (https://tcga-data.nci.nih.gov/docs/publications/lgggbm_2015/). Among them, 103 were identified as IDH mutant on the basis of their genome-wide DNA methylation profile. We classified samples in the validation set using the probes that defined the IDH mutant-specific DNA

methylation cluster analysis integrated in a supervised random forest method. The analysis recapitulated the clusters generated from the TCGA collection (Figure S3C). In order to determine epigenetically regulated (EReg) genes that may be characteristic of the biology of the IDH mutant diffuse glioma subtypes, we compared 450k methylation DNA methylation profiles and gene expression levels between 636 IDH mutant and IDH-wild-type gliomas and 110 non-tumor samples from 11 different tissue types. From the list of epigenetically regulated genes, we extracted 263 genes that were grouped into EReg gene signatures, which showed differential signals among the three IDH mutant subtypes (Figure 3F). These trends were confirmed in the validation set (Figure 3G).

We investigated the possibility that the G-CIMP-high group is a predecessor to the G-CIMP-low group by comparing the DNA methylation profiles from ten IDH mutant-non-codel LGG and GBM primary-recurrent cases with the TCGA cohort. We evaluated the DNA methylation status of probes identified as differentially methylated (n = 90) between G-CIMP-low and G-CIMP-high (FDR < 10^{-13} , difference in mean methylation beta-value > 0.3 and < -0.4). Four out of ten IDHmut-non-codel cases showed a demethylation pattern after disease recurrence, while partial demethylation was demonstrated in the remaining six recurrences, supporting the notion of a progression from G-CIMP-high to G-CIMP-low phenotype (Figure 3H).

An IDH-Wild-Type Subgroup of Histologically Defined Diffuse Glioma Is Associated with Favorable Survival and Shares Epigenomic and Genomic Features with Pilocytic Astrocytoma

IDH-wild-type gliomas segregated into three DNA methylation clusters (Figure S4A). The first is enriched with tumors belonging to the classical gene expression signature and was labeled Classic-like, whereas the second group, enriched with mesenchymal subtype tumors, was labeled Mesenchymal-like (Table S1) (Verhaak et al., 2010). The third cluster contained a larger fraction of LGG in comparison to the other IDH-wild-type clusters. We observed that the IDH-wild-type LGGs but not the IDH-wild-type GBM in this cluster displayed markedly longer survival (log-rank p value = 3.6×10^{-5} ; Figure 4A) and occurred in younger patients (mean 37.6 years versus 50.8 years, t test p value = 0.002). Supervised analysis of differential methylation between LGG and GBM in the third DNA methylation cluster did not reveal any significant probes despite significant differences in stromal content (p value < 0.005; Figure S4D), suggesting that this group cannot be further separated using CpG methylation markers.

Next, we sought to validate the methylation-based classification of IDH-wild-type glioma in an independent cohort of 221 predicted IDH-wild-type glioma samples, including 61 grade I pilocytic astrocytomas (PAs). Toward this aim, we used a supervised random forest model built with the probes that defined the IDH-wild-type clusters. Samples classified as Mesenchymal-like showed enrichment for the Sturm et al. (2012) Mesenchymal subtype (29/88), and gliomas predicted as Classic-like were all RTK II "Classic" (22/22), per the Sturm et al. (2012) classification (Figures 4B and S4B). We observed that PA tumors were unanimously classified as the third,

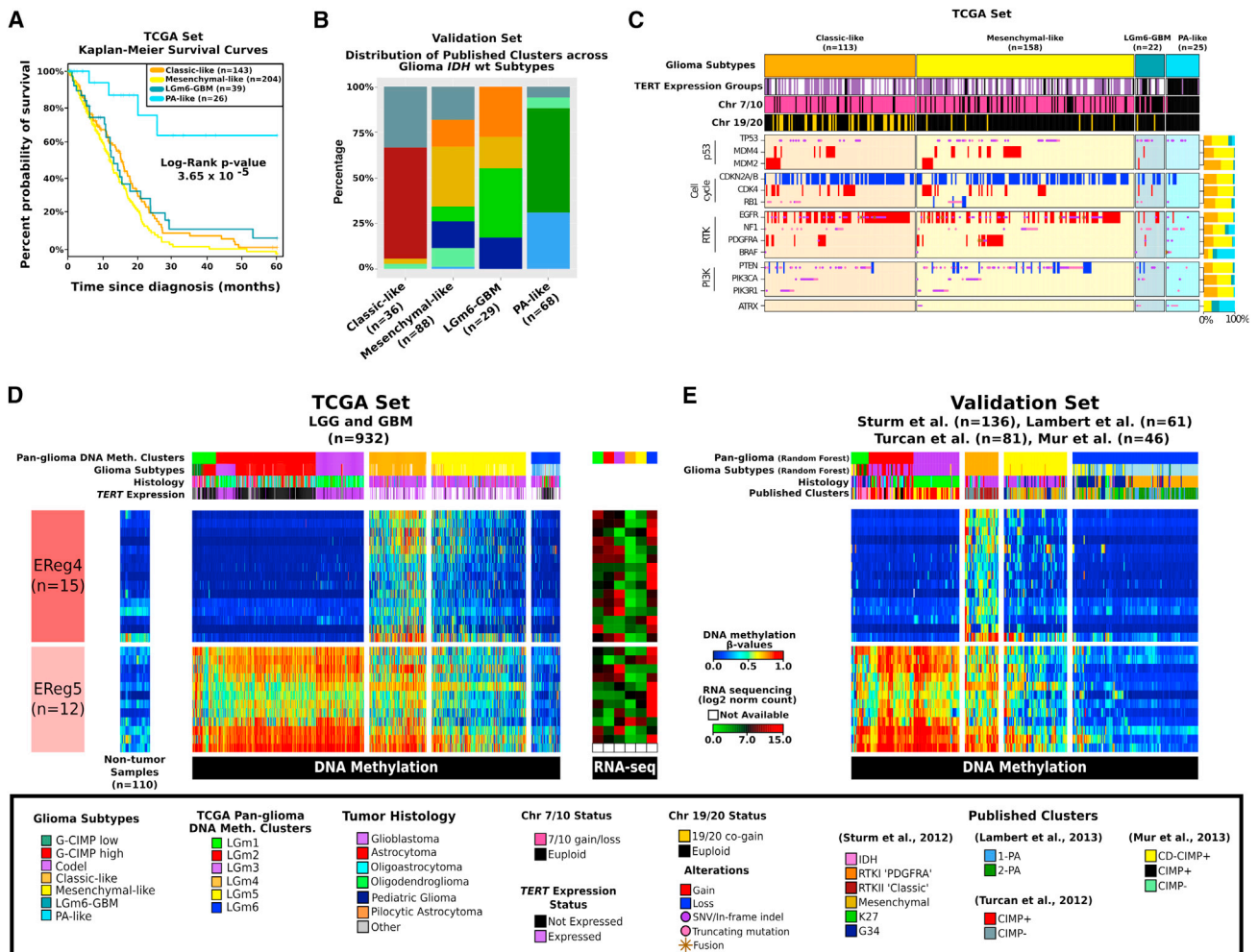


Figure 4. A Distinct Subgroup of IDH-Wild-Type Diffuse Glioma with Molecular Features of Pilocytic Astrocytoma

(A) Kaplan-Meier survival curves for the IDH-wild-type glioma subtypes. Ticks represent censorship. (B) Distribution of previous published DNA methylation subtypes in the validation set, across the TCGA IDH-wild-type-specific DNA methylation clusters. (C) Distribution of genomic alterations in genes frequently altered in IDH-wild-type glioma. (D) Heatmap of TCGA glioma samples ordered according to Figure 2A and two EReg gene signatures defined for the IDH-wild-type DNA methylation clusters. Mean RNA sequencing counts for each gene matched to the promoter of the identified cgID across each cluster are plotted to the right. (E) Heatmap of the validation set classified using the random forest method using the 1,300 probes defined in Figure 2A.

LGG-enriched group (Figure S4B). Based on the molecular similarity with PA, we labeled the LGGs in the third methylation cluster of IDH-wild-type tumors as PA-like. The GBMs in this group were best described as LGM6-GBM for their original pan-glioma methylation cluster assignment and tumor grade.

Pilocytic astrocytomas are characterized by frequent alterations in the MAPK pathway, such as *FGFR1* mutations, *KIAA1549-BRAF*, and *NTRK2* fusions (Jones et al., 2013). The frequency of mutations, fusions, and amplifications in eight PA-associated genes (*BRAF*, *NF1*, *NTRK1*, *NTRK2*, *FGFR1*, and *FGFR2*) rated from 11% (n = 12/113) of Classic-like, 13% (n = 21/158) of Mesenchymal-like IDH-wild-type tumors to 32% (n = 7/22) of LGM6-GBM and 52% (n = 13/25) of PA-like LGG (Fisher's exact test [FET] p value < 0.0001; Figure 4C). Conversely, only 2 of 25 (8%) PA-like LGG tumors showed

TERT expression, compared to 5 of 12 LGM6-GBM (43%), 60 of 65 Classic-like (92%), and 82 of 98 Mesenchymal-like (84%, FET p value < 0.0001). The PA-like group was characterized by relatively low frequency of typical GBM alterations in genes such as *EGFR*, *CDKN2A/B*, and *PTEN* and displayed euploid DNA copy number profiles (Figure S4E). To ascertain that the histologies of the PA-like subgroup had been appropriately classified, we conducted an independent re-review. This analysis confirmed the presence of the histologic features of diffuse glioma (grade II or grade III) in 23 of the 26 cases in the cluster. The remaining three cases were re-named as PA (grade I). An independent review of the magnetic resonance diagnostic images from 13 cases showed a similar pattern, with the majority of tumors showing behavior consistent with grade II or grade III glioma. Taken together, the epigenetic analysis of the

Table 2. DNA Methylation Subtypes Are Prognostically Relevant in Multivariable Analysis and in External Validation Data

		Discovery (n = 809)			Validation (n = 183)		
		C-Index: 0.835 ± 0.019			C-Index: 0.745 ± 0.032		
Predictor	Levels	n	HR (95% CI)	Signif.	n	HR (95% CI)	Signif.
Age at diagnosis	per year	809	1.05 (1.03–1.06)	***	183	1.02 (1–1.04)	*
WHO Grade	II	214	1.0 (ref)		41	1.0 (ref)	
	III	241	1.96 (1.15–3.33)	*	51	1.24 (0.55–2.76)	
	IV	354	2.38 (1.3–4.34)	*	91	2.6 (1.08–6.3)	*
Subgroup	IDHmut-codel	156	1.0 (ref)		57	1.0 (ref)	
	G-CIMP-low	22	5.6 (2.49–12.62)	***	2	0 (0–Inf)	
	G-CIMP-high	219	1.92 (1.05–3.51)	*	15	1.25 (0.43–3.66)	
	classic-like	143	5.4 (2.79–10.44)	***	22	4.55 (1.8–11.49)	*
	mesenchymal-like I	204	8.71 (4.59–16.53)	***	61	5.55 (2.52–12.21)	***
	LGM6-GBM	39	5.79 (2.78–12.1)	***	22	6.8 (2.58–17.91)	**
	PA-like	26	2.02 (0.71–5.71)		4	3.64 (0.79–16.78)	.

Survival regression analysis indicates that an optimal model of prognosis includes age, grade, and methylation subtype. These predictors are statistically significant in both our discovery dataset and an external validation dataset. Significance codes: 0 “****”; 0.001 “***”; 0.05 “**”; 0.1 “.”

IDH-wild-type group of adult glioma revealed the existence of a novel subgroup sharing genetic and DNA methylation features with pediatric PA and favorable clinical outcome compared to diffuse IDH-wild-type glioma. This group may include but extends beyond *BRAF*-mutated grade II oligodendroglioma that were previously recognized as a unique clinical entity (Chi et al., 2013).

Through comparison of the methylation profiles of 636 glioma and 110 non-neoplastic normal samples from different tissue types, we defined EReg signatures consisting of 27 genes that showed differential signals among IDH-wild-type subtypes in the TCGA (Figure 4D) and the validation set (Figure 4E). EReg4 comprised a group of 15 genes hypermethylated and downregulated in particularly Classic-like. EReg5 was defined as a group of 12 genes associated with hypomethylation in LGM6/PA-like compared to all other LGM clusters. These ERegs aided in characterizing the biological importance of IDH-wild-type subtypes and were subsequently used to evaluate the prognostic importance of the IDH-wild-type clusters.

The Epigenetic Classification of Glioma Provides Prognostic Value Independent of Age and Grade

In order to assess whether the DNA methylation-based subtypes we identified carry prognostically relevant information independent of known overall survival predictors, we constructed a series of survival regression models. To find the optimal model for survival prediction, we studied covariates individually and in combination with other covariates. Age at diagnosis, histology, IDH/codel subtype, *TERT* expression, and epigenetic subtype all contribute to survival in single-predictor analysis (log-rank p value < 0.05, Table S4). As expected, age was a highly significant predictor (p < 0.0001, C-Index 0.78) and was included in all subsequent multi-predictor models. We found that histology and grade are highly correlated. Histology provided only marginal improvement to a model that includes grade (likelihood ratio test [LRT] p value = 0.08) and was therefore not included in further analyses. Conversely, grade markedly impacted a histol-

ogy-based predictor model (LRT p value = 0.0005, Table S4) and was retained in the subsequent models. In contrast to previous reports (Eckel-Passow et al., 2015), we failed to observe a statistically significant and independent survival association with *TERT* expression (LRT p value = 0.82, Table S4) or *TERT*p mutations after accounting for age and grade (LRT p value = 0.85, data not shown). Thus, the optimal survival prediction model includes age, grade, and epigenetic subtype (LRT p value < 0.0001, C-Index 0.836; Table 2).

To confirm that the epigenetic subtypes provide independent prognostic information, we tested the survival model on the validation dataset. Epigenetic subtypes in these samples were determined as described above. The distinction between LGM6-GBM and PA-like gliomas was made on the basis of tumor grade and not by DNA methylation signature. Using a subset of 183 samples in the validation cohort with known survival, age, and grade, we found that epigenetic subtypes are significant independent predictors of survival in the multivariate analysis (LRT p value < 0.0001, C-Index 0.746, Table 2). This generalization of our model supports the epigenetic subtypes as a means to improve the prognostication of glioma.

Activation of Cell Cycle/Proliferation and Invasion/Microenvironmental Changes Marks Progression of LGG to GBM

We observed that, in spite of morphological differences between LGG and GBM, such as high cell density and microvascular proliferation, clustering of gene expression profiles frequently grouped LGG and GBM together within the same subtype. Gene Set Enrichment Analysis of the genes activated in G-CIMP GBM as opposed to the IDH mutant-non-codel within LGr3 (Figure 2B) revealed four major groups, including cell cycle and hyperproliferation, DNA metabolic processes, response to stress, and angiogenesis (Figure S5A and Table S5). These biological functions are consistent with the criteria based on mitotic index used by pathologists to discriminate lower and high-grade glioma and the significance of activated microglia for tumor

aggressiveness (Roggendorf et al., 1996). Conversely, compared with the G-CIMP GBM, IDH mutant-non-codel LGG in LGr3 were characterized by enrichment of genes associated with neuro-glial functions such as ion transport and synaptic transmission, possibly suggesting a more differentiated nature. The comparison of co-clustered GBM and LGG in LGr3 by the PARADIGM algorithm that integrates DNA copy number and gene expression to infer pathway activity confirmed that GBMs express genes associated with cell cycle, proliferation, and aggressive phenotype through activation of a number of cell cycle, cell replication, and NOTCH signaling pathways whereas LGGs exhibit an enrichment of neuronal-differentiation-specific categories, including synaptic pathways (Figure S5C and Table S5).

The analysis of the genes activated in GBM versus the LGG component of LGr4, which grouped IDH-wild-type tumors, identified an inflammation and immunologic response signature characterized by the activation of several chemokines (*CCL18*, *CXCL13*, *CXCL2*, and *CXCL3*) and interleukins (*IL8* and *CXCR2*) enriching sets involved in inflammatory and immune response, negative regulation of apoptosis, cell cycle and proliferation, and the I κ B/NF κ B kinase cascade Map (Figure S5B and Table S5). These characteristics suggest differences in the relative amount of microglia. We used the ESTIMATE method to estimate the relative presence of stromal cells, which revealed significantly lower (p value 10^{-6}) stromal scores of LGG IDH-wild-type versus GBM IDH-wild-type (Figure S5F) (Yoshihara et al., 2013). Resembling the functional enrichment for LGG within LGr3, functional enrichment of LGG IDH-wild-type in comparison to GBM within LGr4 showed activation in LGG of special glial-neuronal functions involved in ion transport, synaptic transmission, and nervous system development.

Finally, we aimed to identify transcription factors that may exert control over prominent gene expression programs, known as master regulators. Master regulator analysis comparing the IDH-wild-type group to the IDH mutant group revealed transcription factors that were upregulated in IDH-wild-type gliomas and showed an increase in expression of target genes, including *NKX2-5*, *FOSL1*, *ETV4*, *ETV7*, *RUNX1*, *CEBPB*, *NFE2L3*, *ELF4*, *RUNX3*, *NR2F2*, *PAX8*, and *IRF1* (Table S5). No transcription factors (TFs) were found to be upregulated in IDH mutant gliomas relative to IDH-wild-type gliomas (at a log fold change > 1).

DISCUSSION

This study represents the largest multi-platform genomic analysis performed to date of adult diffuse glioma (WHO grades II, III, and IV). A simplified graphical summary of the identified groups and their main clinical and biological characteristics is reported in Figure 5. The clustering of all diffuse glioma classes and grades within similarly shaped methylation-based and expression-based groups has allowed us to pinpoint specific molecular signatures with clinical relevance. The DNA methylation classification proposed should be considered as a basis and it is likely that future studies involving significantly larger cohorts and more refined profiling methods will be able to further reduce intra-subtype heterogeneity. The dissection of the IDH mutant non-codel G-CIMP LGG and GBM into two separate subgroups (G-CIMP-

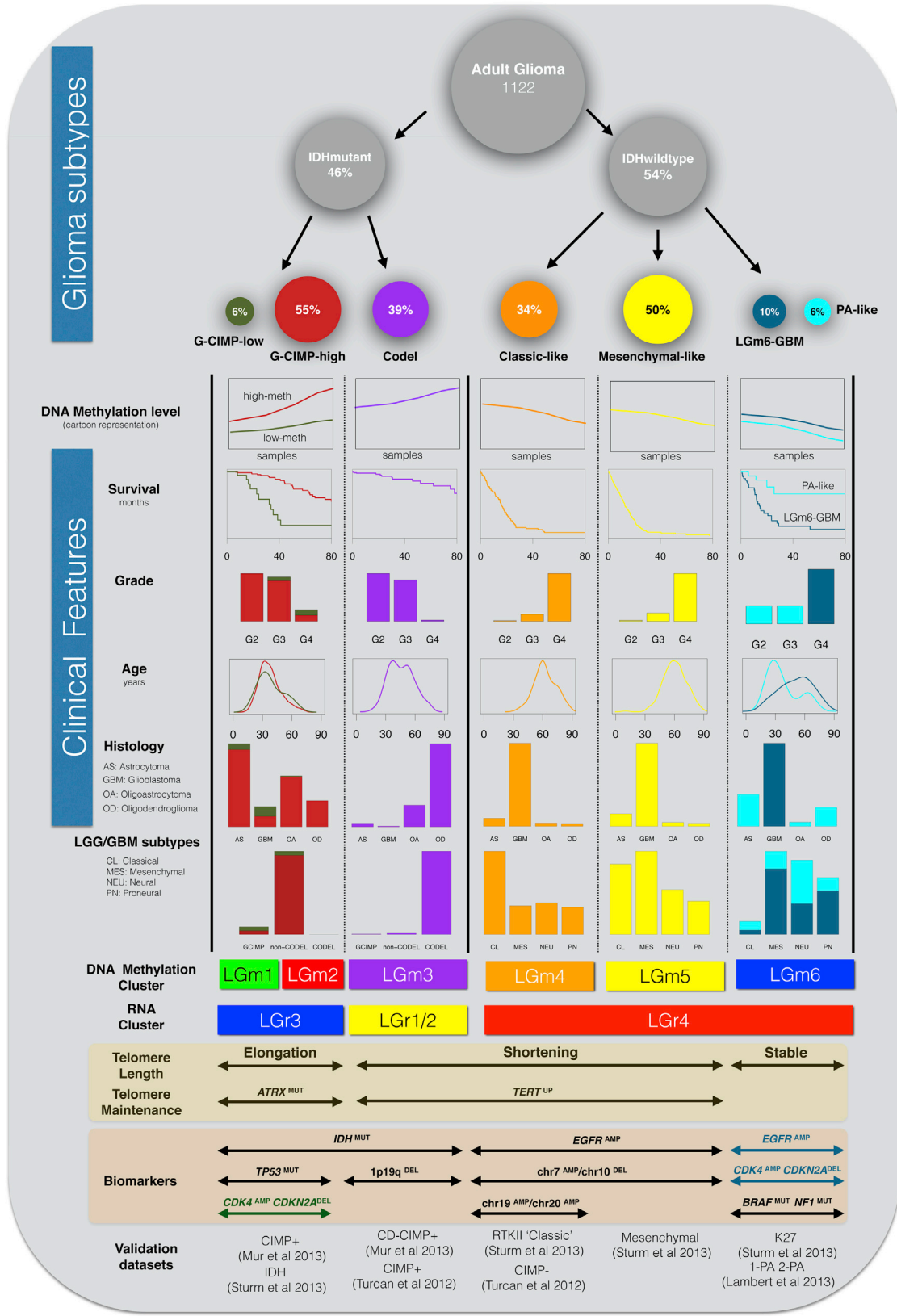
low and G-CIMP-high) based on the extent of genome-wide DNA methylation has crucial biological and clinical relevance. In particular, the identification of the G-CIMP-low subset, characterized by activation of cell cycle genes mediated by SOX binding at hypomethylated functional genomic elements and unfavorable clinical outcome, is an important finding that will guide more accurate segregation and therapeutic assessment in a group of patients in which correlations of conventional grading with outcome are modest (Olar et al., 2015; Reuss et al., 2015). The finding that G-CIMP-high tumors can emerge as G-CIMP-low glioma at recurrence identifies variations in DNA methylation as crucial determinants for glioma progression and provides a clue to the mechanisms driving evolution of glioma. Our results unify previous observations that linked the cell cycle pathway to malignant progression of low-grade glioma (Mazor et al., 2015). Future updates of the TCGA glioma clinical annotation and independent validation of our findings may be able to consider additionally important clinical confounders such as extent of resection and performance status to further optimize the weights of the currently known prognostic variables and their association to the molecular subtypes we identified.

Analysis of IDH-wild-type glioma revealed the PA-like LGG subset that harbors a silent genomic landscape, confers favorable prognosis relative to other IDH-wild-type diffuse glioma, and displays a molecular profile with high similarity to PA. Re-view by neuropathologists and neuroradiologists confirmed that the majority were correctly diagnosed as diffuse glioma, emphasizing the need for integration of molecular signatures into clinical classification (Chi et al., 2013) for this subgroup of patients that may be spared potentially unnecessary intensive treatments.

The large number of exomes in our dataset allowed identification of novel glioma-associated somatic alterations, including in the *KRAS* and *NRAS* genes, which were frequently used in genetically engineered glioma mouse models (Holland et al., 2000). Our analysis further nominates glial tumors to join an increasing number of tumor types characterized by a deactivated cohesin pathway (Kon et al., 2013; Solomon et al., 2011). Cohesin mutant tumors may infer increased sensitivity to DNA damage agents and PARP inhibitors (Bailey et al., 2014), suggesting that gliomas with genetic alterations of key cohesin regulatory factors may represent biomarkers and therapeutic opportunities.

Overexpression of *TERT* mRNA was found to be associated with increased telomere length in urothelial cancer (Borah et al., 2015). Our results revealed that, in gliomas, increased telomere length is associated with *ATRX* mutations, suggesting an alternative lengthening of telomeres (ALT) mechanism. ALT has been associated with sensitivity to inhibition of the protein kinase ATR (Flynn et al., 2015).

In summary, our pan-glioma analysis has expanded our knowledge of the glioma somatic alteration landscape, emphasized the relevance of DNA methylation profiles as a modality for clinical classification, and quantitatively linked somatic *TERT* pathway alterations to telomere maintenance. Combined, these findings are an important step forward in our understanding of glioma as discrete disease subsets and the mechanisms driving gliomagenesis.



(legend on next page)

EXPERIMENTAL PROCEDURES

Patient and Sample Characteristics

Specimens were obtained from patients with appropriate consent from institutional review boards. Details of sample preparation are described in the [Supplemental Experimental Procedures](#).

Data Generation

In total, tumors from 1,132 patients were assayed on at least one molecular profiling platform, which platforms included: (1) whole-genome sequencing, including high coverage and low pass whole-genome sequencing; (2) exome sequencing; (3) RNA sequencing; (4) DNA copy-number and single-nucleotide polymorphism arrays, including Agilent CGH 244K, Affymetrix SNP6.0, and Illumina 550K Infinium HumanHap550 SNP Chip microarrays; (5) gene expression arrays, including Agilent 244K Custom Gene Expression, Affymetrix HT-HGU133A and Affymetrix Human Exon 1.0 ST arrays; (6) DNA methylation arrays, including Illumina GoldenGate Methylation, Illumina Infinium HumanMethylation27, and Illumina Infinium HumanMethylation450 Bead-Chips; (7) reverse phase protein arrays; (8) miRNA sequencing; and (9) miRNA Agilent 8 × 15K Human miRNA-specific microarrays. Details of data generation have been previously reported ([Brennan et al., 2013](#); [Cancer Genome Atlas Research Network et al., 2015](#)). To ensure cross-platform comparability, features from all array platforms were compared to a reference genome.

Data Analysis

The data and analysis results can be explored through the Broad Institute FireBrowse portal (<http://firebrowse.org/?cohort=GBMLGG>), the cBioPortal for Cancer Genomics (http://www.cbioportal.org/study.do?cancer_study_id=lgggbm_tcga_pub), in a Tumor Map (<http://tumormap.ucsc.edu/?p=newton.gliomas-paper>), the TCGA transcript fusion portal (<http://www.tumorfusions.org>), TCGA Batch Effects (<http://bioinformatics.mdanderson.org/tcgambatch/>), Regulome Explorer (<http://explorer.cancerregulome.org/>), Next-Generation Clustered Heat Maps (<http://bioinformatics.mdanderson.org/TCGA/NGCHMPortal/>). See also [Supplemental Information](#) and the TCGA publication page (https://tcga-data.nci.nih.gov/docs/publications/lgggbm_2015/).

SUPPLEMENTAL INFORMATION

Supplemental Information includes Supplemental Experimental Procedures, five figures, and five tables and can be found with this article online at <http://dx.doi.org/10.1016/j.cell.2015.12.028>.

AUTHOR CONTRIBUTIONS

Conceptualization and project administration: R.G.W.V., A.I., and H.N.; supervision: S.R.S., K.D.A., P.W.L., M.G., D.H., D.J.B., D.H.G., R.R., C.C.L., J.S.B.-S., C.G.C., D.P.C.T., W.K.A.Y., J.H., L.C., M.M., and T.M.; formal analysis: R.G.W.V., A.I., H.N., M.C., F.P.B., T.M.M., T.S.S., O.M., Y.N., S.M.P., P.Z., L.P., A. Radenbaugh, G.R., R.A., J.W., G.M., S.L., S.A., A. Rao, B.A.M., A.D.C., and H.Z.; investigation: D.J.B., L.C., and L.P.; data curation: D.J.B., L.P., and F.P.B.; writing - original draft: R.G.W.V., A.I., H.N., M.C., F.P.B., T.M.M., and T.S.S.; manuscript review: D.J.B., K.A.D., S.R.S., M.W., N.L., and D.H.G.

ACKNOWLEDGMENTS

This study was supported by NIH grants U24CA143883, U24CA143858, U24CA143840, U24CA143799, U24CA143835, U24CA143845,

U24CA143882, U24CA143867, U24CA143866, U24CA143848, U24CA144025, U54HG003067, U54HG003079, U54HG003273, U24CA126543, U24CA126544, U24CA126546, U24CA126551, U24CA126554, U24CA126561, U24CA126563, U24CA143731, U24CA143843, P30CA016672, P50 CA127001, U54CA193313, R01CA179044, R01CA185486, R01 CA190121, and P01 CA085878; Cancer Prevention & Research Institute of Texas (CPRI) R140606; and São Paulo Research Foundation (FAPESP) 2014/02245-3, 2015/07925-5, 2015/02844-7, and 2015/08321-3. D.J.W. is a consultant for Zymo Research Corporation. R.B. is a consultant for and received grant funding from Novartis. A.D.C. and M.M. received grant support from Bayer.

Received: July 17, 2015

Revised: October 20, 2015

Accepted: December 11, 2015

Published: January 28, 2016

REFERENCES

- Bailey, M.L., O'Neil, N.J., van Pel, D.M., Solomon, D.A., Waldman, T., and Hietter, P. (2014). Glioblastoma cells containing mutations in the cohesin component STAG2 are sensitive to PARP inhibition. *Mol. Cancer Ther.* *13*, 724–732.
- Berman, B.P., Weisenberger, D.J., Aman, J.F., Hinoue, T., Ramjan, Z., Liu, Y., Noushmehr, H., Lange, C.P., van Dijk, C.M., Tollenaar, R.A., et al. (2012). Regions of focal DNA hypermethylation and long-range hypomethylation in colorectal cancer coincide with nuclear lamina-associated domains. *Nat. Genet.* *44*, 40–46.
- Borah, S., Xi, L., Zaugg, A.J., Powell, N.M., Dancik, G.M., Cohen, S.B., Costello, J.C., Theodorescu, D., and Cech, T.R. (2015). Cancer. TERT promoter mutations and telomerase reactivation in urothelial cancer. *Science* *347*, 1006–1010.
- Brennan, C.W., Verhaak, R.G., McKenna, A., Campos, B., Noushmehr, H., Salama, S.R., Zheng, S., Chakravarty, D., Sanborn, J.Z., Berman, S.H., et al.; TCGA Research Network (2013). The somatic genomic landscape of glioblastoma. *Cell* *155*, 462–477.
- Cancer Genome Atlas Research Network, Brat, D.J., Verhaak, R.G., Aldape, K.D., Yung, W.K., Salama, S.R., Cooper, L.A., Rheinbay, E., Miller, C.R., Vitucci, M., et al. (2015). Comprehensive, integrative genomic analysis of diffuse lower-grade gliomas. *N. Engl. J. Med.* *372*, 2481–2498.
- Chi, A.S., Batchelor, T.T., Yang, D., Dias-Santagata, D., Borger, D.R., Ellisen, L.W., Iafra, A.J., and Louis, D.N. (2013). BRAF V600E mutation identifies a subset of low-grade diffusely infiltrating gliomas in adults. *J. Clin. Oncol.* *31*, e233–e236.
- Eckel-Passow, J.E., Lachance, D.H., Molinaro, A.M., Walsh, K.M., Decker, P.A., Sicotte, H., Pekmezci, M., Rice, T., Kosel, M.L., Smirnov, I.V., et al. (2015). Glioma Groups Based on 1p/19q, IDH, and TERT Promoter Mutations in Tumors. *N. Engl. J. Med.* *372*, 2499–2508.
- Flynn, R.L., Cox, K.E., Jeitany, M., Wakimoto, H., Bryll, A.R., Ganem, N.J., Bersani, F., Pineda, J.R., Suvà, M.L., Benes, C.H., et al. (2015). Alternative lengthening of telomeres renders cancer cells hypersensitive to ATR inhibitors. *Science* *347*, 273–277.
- Frattoni, V., Trifonov, V., Chan, J.M., Castano, A., Lia, M., Abate, F., Keir, S.T., Ji, A.X., Zoppi, P., Niola, F., et al. (2013). The integrated landscape of driver genomic alterations in glioblastoma. *Nat. Genet.* *45*, 1141–1149.
- Graham, V., Khudyakov, J., Ellis, P., and Pevny, L. (2003). SOX2 functions to maintain neural progenitor identity. *Neuron* *39*, 749–765.

Figure 5. Overview of Major Subtypes of Adult Diffuse Glioma

Integrative analysis of 1,122 adult gliomas resulted in 7 different subtypes with distinct biological and clinical characteristics. The groups extend across six DNA methylation subtypes of which the LGM6 cluster was further separated by tumor grade into PA-like and LGM6-GBM. The size of the circles is proportional to the percentages of samples within each group. DNA methylation plot is a cartoon representation of overall genome-wide epigenetic pattern within glioma subtypes. Survival information is represented as a set of Kaplan-Meier curves, counts of grade, histology and LGG/GBM subtypes within the groups are represented as bar-plots, whereas age is represented as density. Labeling of telomere length and maintenance status is based on the enrichment of samples within each column, similarly for the biomarkers and the validation datasets.

- Guintivano, J., Aryee, M.J., and Kaminsky, Z.A. (2013). A cell epigenotype specific model for the correction of brain cellular heterogeneity bias and its application to age, brain region and major depression. *Epigenetics* 8, 290–302.
- Holland, E.C., Celestino, J., Dai, C., Schaefer, L., Sawaya, R.E., and Fuller, G.N. (2000). Combined activation of Ras and Akt in neural progenitors induces glioblastoma formation in mice. *Nat. Genet.* 25, 55–57.
- Horn, S., Figl, A., Rachakonda, P.S., Fischer, C., Sucker, A., Gast, A., Kadel, S., Moll, I., Nagore, E., Hemminki, K., et al. (2013). TERT promoter mutations in familial and sporadic melanoma. *Science* 339, 959–961.
- Jones, D.T., Hutter, B., Jäger, N., Korshunov, A., Kool, M., Warnatz, H.J., Zichner, T., Lambert, S.R., Ryzhova, M., Quang, D.A., et al.; International Cancer Genome Consortium PedBrain Tumor Project (2013). Recurrent somatic alterations of FGFR1 and NTRK2 in pilocytic astrocytoma. *Nat. Genet.* 45, 927–932.
- Killela, P.J., Reitman, Z.J., Jiao, Y., Bettegowda, C., Agrawal, N., Diaz, L.A., Jr., Friedman, A.H., Friedman, H., Gallia, G.L., Giovanella, B.C., et al. (2013). TERT promoter mutations occur frequently in gliomas and a subset of tumors derived from cells with low rates of self-renewal. *Proc. Natl. Acad. Sci. USA* 110, 6021–6026.
- Kim, H., Zheng, S., Amini, S.S., Virk, S.M., Mikkelsen, T., Brat, D.J., Grimsby, J., Sougnez, C., Muller, F., Hu, J., et al. (2015). Whole-genome and multisector exome sequencing of primary and post-treatment glioblastoma reveals patterns of tumor evolution. *Genome Res.* 25, 316–327.
- Kon, A., Shih, L.Y., Minamino, M., Sanada, M., Shiraishi, Y., Nagata, Y., Yoshida, K., Okuno, Y., Bando, M., Nakato, R., et al. (2013). Recurrent mutations in multiple components of the cohesin complex in myeloid neoplasms. *Nat. Genet.* 45, 1232–1237.
- Kurscheid, S., Bady, P., Sciuscio, D., Samarzija, I., Shay, T., Vassallo, I., Criecking, W.V., Daniel, R.T., van den Bent, M.J., Marosi, C., et al. (2015). Chromosome 7 gain and DNA hypermethylation at the HOXA10 locus are associated with expression of a stem cell related HOX-signature in glioblastoma. *Genome Biol.* 16, 16.
- Lambert, S.R., Witt, H., Hovestadt, V., Zucknick, M., Kool, M., Pearson, D.M., Korshunov, A., Ryzhova, M., Ichimura, K., Jabado, N., et al. (2013). Differential expression and methylation of brain developmental genes define location-specific subsets of pilocytic astrocytoma. *Acta Neuropathol.* 126, 291–301.
- Lodato, M.A., Ng, C.W., Wamstad, J.A., Cheng, A.W., Thai, K.K., Fraenkel, E., Jaenisch, R., and Boyer, L.A. (2013). SOX2 co-occupies distal enhancer elements with distinct POU factors in ESCs and NPCs to specify cell state. *PLoS Genet.* 9, e1003288.
- Louis, D.N., Ohgaki, H., Wiestler, O.D., Cavenee, W.K., Burger, P.C., Jouvet, A., Scheithauer, B.W., and Kleihues, P. (2007). The 2007 WHO classification of tumours of the central nervous system. *Acta Neuropathol.* 114, 97–109.
- Mazor, T., Pankov, A., Johnson, B.E., Hong, C., Hamilton, E.G., Bell, R.J., Smirnov, I.V., Reis, G.F., Phillips, J.J., Barnes, M.J., et al. (2015). DNA Methylation and Somatic Mutations Converge on the Cell Cycle and Define Similar Evolutionary Histories in Brain Tumors. *Cancer Cell* 28, 307–317.
- Mur, P., Mollejo, M., Ruano, Y., de Lope, A.R., Fiaño, C., García, J.F., Castresana, J.S., Hernández-Laín, A., Rey, J.A., and Meléndez, B. (2013). Codeletion of 1p and 19q determines distinct gene methylation and expression profiles in IDH-mutated oligodendroglial tumors. *Acta Neuropathol.* 126, 277–289.
- Noushmehr, H., Weisenberger, D.J., Diefes, K., Phillips, H.S., Pujara, K., Berman, B.P., Pan, F., Pelloski, C.E., Sulman, E.P., Bhat, K.P., et al.; Cancer Genome Atlas Research Network (2010). Identification of a CpG island methylator phenotype that defines a distinct subgroup of glioma. *Cancer Cell* 17, 510–522.
- Olar, A., Wani, K.M., Alfaro-Munoz, K.D., Heathcock, L.E., van Thuijl, H.F., Gilbert, M.R., Armstrong, T.S., Sulman, E.P., Cahill, D.P., Vera-Bolanos, E., et al. (2015). IDH mutation status and role of WHO grade and mitotic index in overall survival in grade II-III diffuse gliomas. *Acta Neuropathol.* 129, 585–596.
- Ozawa, T., Riester, M., Cheng, Y.K., Huse, J.T., Squatrito, M., Helmy, K., Charles, N., Michor, F., and Holland, E.C. (2014). Most human non-GCIMP glioblastoma subtypes evolve from a common proneural-like precursor glioma. *Cancer Cell* 26, 288–300.
- Peters, J.M., and Nishiyama, T. (2012). Sister chromatid cohesion. *Cold Spring Harb. Perspect. Biol.* 4, a011130.
- Pineda, C.T., Ramanathan, S., Fon Tacer, K., Weon, J.L., Potts, M.B., Ou, Y.H., White, M.A., and Potts, P.R. (2015). Degradation of AMPK by a cancer-specific ubiquitin ligase. *Cell* 160, 715–728.
- Reuss, D.E., Mamatjan, Y., Schrimpf, D., Capper, D., Hovestadt, V., Kratz, A., Sahm, F., Koelsche, C., Korshunov, A., Olar, A., et al. (2015). IDH mutant diffuse and anaplastic astrocytomas have similar age at presentation and little difference in survival: a grading problem for WHO. *Acta Neuropathol.* 129, 867–873.
- Roggendorf, W., Strupp, S., and Paulus, W. (1996). Distribution and characterization of microglia/macrophages in human brain tumors. *Acta Neuropathol.* 92, 288–293.
- Schwartzbaum, J.A., Fisher, J.L., Aldape, K.D., and Wrensch, M. (2006). Epidemiology and molecular pathology of glioma. *Nat. Clin. Pract. Neurol.* 2, 494–503.
- Solomon, D.A., Kim, T., Diaz-Martinez, L.A., Fair, J., Elkhouloun, A.G., Harris, B.T., Toretsky, J.A., Rosenberg, S.A., Shukla, N., Ladanyi, M., et al. (2011). Mutational inactivation of STAG2 causes aneuploidy in human cancer. *Science* 333, 1039–1043.
- Sturm, D., Witt, H., Hovestadt, V., Khuong-Quang, D.A., Jones, D.T., Konermann, C., Pfaff, E., Tönjes, M., Sill, M., Bender, S., et al. (2012). Hotspot mutations in H3F3A and IDH1 define distinct epigenetic and biological subgroups of glioblastoma. *Cancer Cell* 22, 425–437.
- Sturm, D., Bender, S., Jones, D.T., Lichter, P., Grill, J., Becher, O., Hawkins, C., Majewski, J., Jones, C., Costello, J.F., et al. (2014). Paediatric and adult glioblastoma: multifactorial (epi)genomic culprits emerge. *Nat. Rev. Cancer* 14, 92–107.
- Suvà, M.L., Rheinbay, E., Gillespie, S.M., Patel, A.P., Wakimoto, H., Rabkin, S.D., Riggi, N., Chi, A.S., Cahill, D.P., Nahed, B.V., et al. (2014). Reconstructing and reprogramming the tumor-propagating potential of glioblastoma stem-like cells. *Cell* 157, 580–594.
- Suzuki, H., Aoki, K., Chiba, K., Sato, Y., Shiozawa, Y., Shiraishi, Y., Shimamura, T., Niida, A., Motomura, K., Ohka, F., et al. (2015). Mutational landscape and clonal architecture in grade II and III gliomas. *Nat. Genet.* 47, 458–468.
- Turcan, S., Rohle, D., Goenka, A., Walsh, L.A., Fang, F., Yilmaz, E., Campos, C., Fabius, A.W., Lu, C., Ward, P.S., et al. (2012). IDH1 mutation is sufficient to establish the glioma hypermethylator phenotype. *Nature* 483, 479–483.
- van den Bent, M.J. (2010). Interobserver variation of the histopathological diagnosis in clinical trials on glioma: a clinician's perspective. *Acta Neuropathol.* 120, 297–304.
- Verhaak, R.G., Hoadley, K.A., Purdom, E., Wang, V., Qi, Y., Wilkerson, M.D., Miller, C.R., Ding, L., Golub, T., Mesirov, J.P., et al.; Cancer Genome Atlas Research Network (2010). Integrated genomic analysis identifies clinically relevant subtypes of glioblastoma characterized by abnormalities in PDGFRA, IDH1, EGFR, and NF1. *Cancer Cell* 17, 98–110.
- Yan, H., Parsons, D.W., Jin, G., McLendon, R., Rasheed, B.A., Yuan, W., Kos, I., Batonic-Haberle, I., Jones, S., Riggins, G.J., et al. (2009). IDH1 and IDH2 mutations in gliomas. *N. Engl. J. Med.* 360, 765–773.
- Yoshihara, K., Shahmoradgoli, M., Martínez, E., Vegesna, R., Kim, H., Torres-García, W., Treviño, V., Shen, H., Laird, P.W., Levine, D.A., et al. (2013). Inferring tumour purity and stromal and immune cell admixture from expression data. *Nat. Commun.* 4, 2612.